AGU PUBLICATIONS

Geophysical Research Letters

RESEARCH LETTER
10.1002/2017GL073949

Key Points:
- b_{bp} (700) values at 900-950 m are nearly constant in most areas of the oceans
- Seasonality is observed at high latitudes, and higher values are observed in association with significant O_2 minimum zones
- Values are consistent with measurements of suspended particulate concentrations performed in the 70s

Correspondence to:
A. Poteau,
antoine.poteau@upmc.fr

Citation:
Poteau, A., E. Boss, and H. Claustre (2017), Particulate concentration and seasonal dynamics in the mesopelagic ocean based on the backscattering coefficient measured with Biogeochemical-Argo floats, *Geophys. Res. Lett.*, *44*, 6933–6939, doi:10.1002/2017GL073949.

Received 24 APR 2017
Accepted 22 JUN 2017
Accepted article online 26 JUN 2017
Published online 12 JUL 2017

Particulate concentration and seasonal dynamics in the mesopelagic ocean based on the backscattering coefficient measured with Biogeochemical-Argo floats

Antoine Poteau[1], **Emmanuel Boss**[2], **and Hervé Claustre**[1]

[1] Laboratoire d'Océanographie de Villefranche (LOV), Sorbonne Universités, 5 UPMC Univ Paris 06, CNRS, UMR 7093, Villefranche-sur-mer, France, [2] School of Marine Sciences, University of Maine, Orono, Maine, USA

Abstract We explore a novel and spatially extensive data set obtained from Biogeochemical-Argo (or BGC-Argo) floats, containing 16,796 profiles of the particulate backscattering coefficient at 700 nm (b_{bp}(700)) measured with three different sensors. We focus at the 900–950m depth interval (within the mesopelagic), where we found values to be relatively constant. While we find significant differences between estimates of b_{bp}(700) obtained with different sensors (≈30% disagreement), the median values in most oceanic regions obtained with a single type of sensor are within 50% of each other and are consistent with measurements of suspended mass conducted in the early 1970s. Deviations from the quasi-constant background value likely indicate times and locations associated with higher particulate export to depth. Indeed, we observe that in productive high-latitude regions, a deep seasonal signal is observed, with enhanced values recorded a few months after surface spring/summer maximal concentrations. In addition, the deep b_{bp}(700) is highest in regions exhibiting suboxic-anoxic conditions (e.g., Northern Indian Ocean), which have been associated with local particulate production as well as reduced particle flux attenuation.

1. Introduction

The concentration of particles in a given layer below the productive sunlit surface layer of the oceans reflects a balance between supply (e.g., sinking of particles from above, aggregation, and local release of fecal pellets), sinking to depth, and local respiration (e.g., consumption by bacteria and other organisms). Since these processes regulate one of the main processes contributing to the sequestration of atmospheric carbon dioxide into the deep ocean, it is of great interest to be able to monitor the concentration and dynamics of particles at depth. To date, monitoring particle concentrations in the mesopelagic has been conducted using research vessels and the maintenance of a few long-term time series (e.g., the Bermuda and Hawaii time series). Back in the 1970s, the Geochemical Ocean Sections Study program performed basin-scale sampling to map the distribution of particulate material throughout ocean basins [*Brewer et al.*, 1976]. Filtration of large water samples were used initially but provided poor vertical resolution. Introduction of optical technology, the forward-scattering measurements using Nephlometers, provided high vertical resolution of particulate distribution based on the derivation of proxy relation between particulate mass and scattering [*Ewing and Thorndike*, 1965a; *Biscaye and Eittreim*, 1977]. Side scattering sensors have been used on profiling floats since 2004 [*Boss et al.*, 2008] and were later replaced by backscattering sensors [e.g., *Whitmire et al.*, 2009]. These sensors have become ubiquitous on profiling floats since 2010, and there are currently more than 130 floats with such sensors profiling the world's ocean. In this paper we present evidence that optical measurements done using autonomous profiling floats equipped with a backscattering sensor provide quantitative information on the distribution and seasonal dynamics of particulate material concentration in these extremely clear waters.

2. Methods

2.1. Data Source

All the data used in this manuscript come from Argo Global Data Assembly Center (ftp://ftp.ifremer.fr/ifremer/argo) and correspond to all the data available as of 31 December 2016 from a snapshot of Argo GDAC

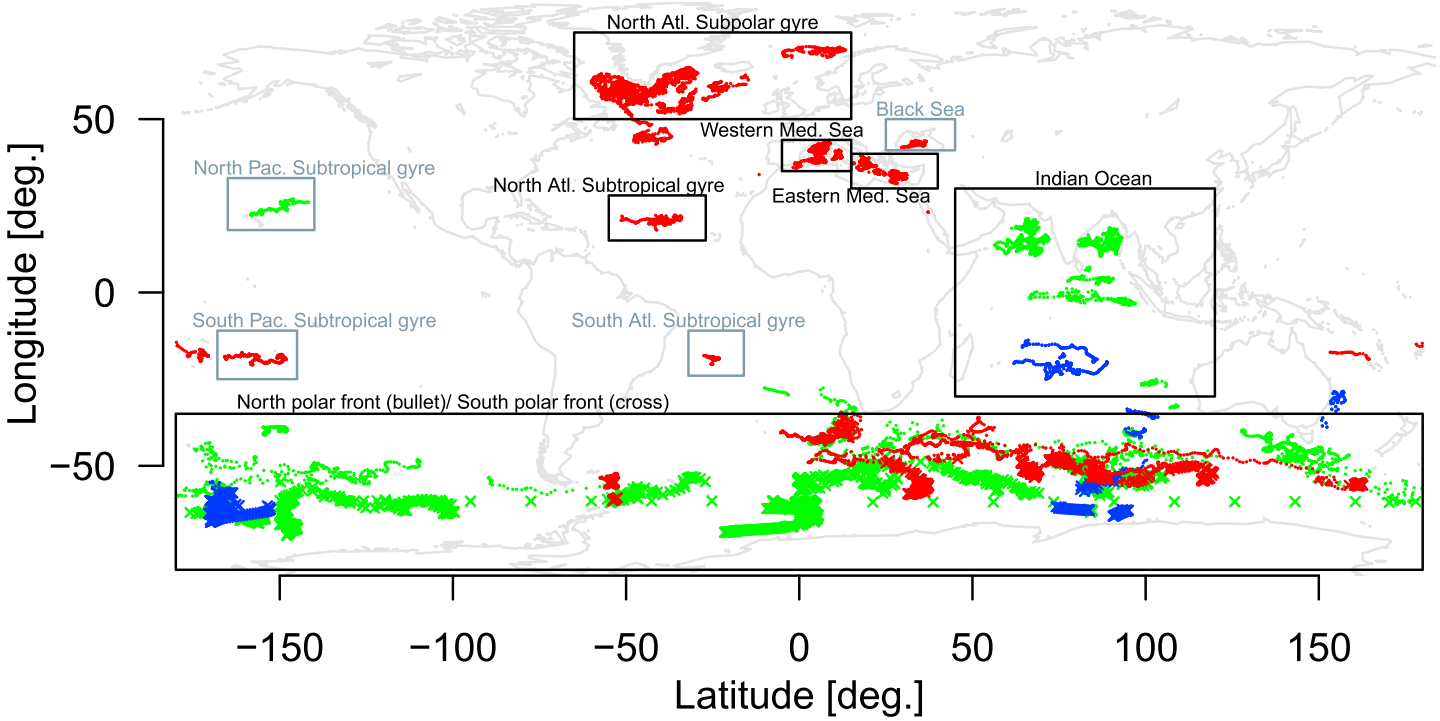

Figure 1. Geographical distribution of all $b_{bp}(700)$ data analyzed in this study. They are colored based on the technology used, Eco-Triplet 124° in red, Eco-FLBB 142° in green, and MCOMS 149° in blue. Black rectangles designate zones in which sufficient floats and profiles exist to perform zonal analysis. The Southern Ocean was further separated into two zones, north and south (identified by crosses) of the Polar Front.

[*Argo*, 2017]. This data set includes data collected from September 2010 to December 2016. It involves a variety of float platforms (NKE's PROVOR, Webb's APEX, and SeaBird's NAVIS) performing different missions (in dive depths, frequency of profiling, and data acquisition) and equipped with different sensors for backscattering at 700 nm (Seabird MCOMS, WETLabs Eco-Triplet, and Eco-FLBB). Those sensors differ in measurement angle (nominal angles of scattering are 149°, 124°, and 142°, respectively (Figure 1 and Table 1)).

2.2. Particulate Backscattering Data

The data used are all derived particulate backscattering coefficients at 700 nm measured between 900 and 950 m all taken, while the float is profiling in the ascent mode (some floats collect data in drift mode which we do not use here). The particulate backscattering coefficient in this database is computed following the methodology described in *Schmechtig et al.* [2015]. However, it is important to mention here two sources of uncertainties: (1) the dark current value used in the computation of the backscattering and (2) the $\chi(\theta)$ factor which is used to convert angular scattering measurements (known as the volume scattering function) performed at an angular range around a specific angle, θ, to the (hemispherical) backscattering coefficient (we use values provided in *Sullivan et al.* [2013]). We found a total of 21,283 distinct profiles from 248 different floats with $b_{bp}(700)$ data between 900 and 950 m and computed the median for each profiles. To avoid contamination with detached nepheloid layers [e.g., *Gardner et al.*, 2017], we only use data where depth is deeper than 2000 m, reducing our data set by 2566 $b_{bp}(700)$ values. We visually inspected all the times series. For 22 floats we identified fouling of sensors sometime along the time series and removed all the values at and following where we identified a monotonic rise in backscattering at depth, reducing further our data set by 1920 $b_{bp}(700)$ values. Additionally, we removed one negative outlier. After those procedures were applied, the final data set comprises 16,796 $b_{bp}(700)$ values between 900 and 950 m. We quantify the variability at the basin-scale data by computing the "spread" defined as (84th−16th percentile)/2, equivalent to the standard deviation for the normally distributed data. For monthly climatologies we further divide the spread by N, which corresponds to the number of floats associated to each monthly calculation, hence obtaining the "spread of the median." This is equivalent to a standard error of the mean for a normally distributed variable, where we consider each float to provide an independent realization.

Geophysical Research Letters

10.1002/2017GL073949

Table 1. Number of Independent Floats, Number of Profiles (Minimum Number of Floats (*N*) and Profiles at a Given Month), With Specific Sensors (Eco-Triplet, Eco-FLBB, and MCOMS), Their Median and Spread for Specific Regions[a]

	Eco-Triplet 124°		Eco-FLBB 142°		MCOMS 149°	
Region	nb. floats / nb. prof. (min(floats. month^{-1})/ min(prof. month^{-1}))	Median b_{bp}(700) (m^{-1}) (spread)	nb. floats / nb. prof. (min(floats. month^{-1})/ min(prof. month^{-1}))	Median b_{bp}(700) (m^{-1}) (spread)	nb. floats / nb. prof. (min(floats. month^{-1})/ min(prof. month^{-1}))	Median b_{bp}(700) (m^{-1}) (spread)
North Atl. Subpolar gyre	20 / 2807 (13 / 141)	$1.7\ 10^{-4}$ ($0.5\ 10^{-4}$)	-	-	-	-
North Polar Front	16 / 1977 (11 / 103)	$2\ 10^{-4}$ ($0.5\ 10^{-4}$)	36 / 1900 (20 / 124)	$2.9\ 10^{-4}$ ($0.65\ 10^{-4}$)	5 / 207 (2 / 7)	$3.6\ 10^{-4}$ ($0.6\ 10^{-4}$)
South Polar Front	15 / 653 (3 / 10)	$1.7\ 10^{-4}$ ($0.6\ 10^{-4}$)	30 / 1215 (17 / 78)	$2.4\ 10^{-4}$ ($1\ 10^{-4}$)	8 / 194 (3 / 4)	$2.4\ 10^{-4}$ ($0.6\ 10^{-4}$)
Black sea	3 / 214 (1 / 10)	$4\ 10^{-4}$ ($0.5\ 10^{-4}$)	-	-	-	-
North Atl. Subtropical gyre	4 / 413 (3 / 22)	$1.5\ 10^{-4}$ ($0.2\ 10^{-4}$)	-	-	-	-
North Pac. Subtropical gyre	-	-	1/218 (1 / 16)	$2.2\ 10^{-4}$ ($0.2\ 10^{-4}$)	-	-
South Alt. Subtropical gyre	4 / 169 (1 / 5)	$1.3\ 10^{-4}$ ($0.3\ 10^{-4}$)	-	-	-	-
South Pac. Subtropical gyre	4 / 448 (2 / 12)	$1.5\ 10^{-4}$ ($0.3\ 10^{-4}$)	-	-	-	-
Indian Ocean	-	-	33 / 2046 (19 / 144)	$3.3\ 10^{-4}$ ($0.8\ 10^{-4}$)	4 / 762 (3 / 18)	$2.4\ 10^{-4}$ ($0.3\ 10^{-4}$)
Eastern Med. Sea	16 / 1438 (10 / 95)	$2\ 10^{-4}$ ($0.4\ 10^{-4}$)	-	-	-	-
Western Med. Sea	20 / 1603 (10 / 103)	$2\ 10^{-4}$ ($0.4\ 10^{-4}$)	-	-	-	-
Other	6 / 388 (2 / 16)	$1.8\ 10^{-4}$ ($0.42\ 10^{-4}$)	3 / 89 (0 / 0)	$5\ 10^{-4}$ ($2.3\ 10^{-4}$)	2 / 124 (0 / 0)	$2.9\ 10^{-4}$ ($0.28\ 10^{-4}$)
All	96 / 10110 (64 / 658)	$1.8\ 10^{-4}$ ($0.5\ 10^{-4}$)	89 / 5399 (55 / 373)	$3\ 10^{-4}$ ($0.85\ 10^{-4}$)	15 / 1287 (9 / 61)	$2.5\ 10^{-4}$ ($0.45\ 10^{-4}$)

[a]The meaning of the blue data in the table body is explained by the blue portions of the first, third, and fifth column headings.

Table 2. Statistics for Zones in Which at Least 10 Profiles From Three Distinct Floats Per Month Were Available, Also Used to Derive the Seasonal Dynamics in Figure 3

	Eco-Triplet 124°	Eco-FLBB 142°	MCOMS 149°
Zone	Median $b_{bp}(700)$ (spread)	Median $b_{bp}(700)$ (spread)	Median $b_{bp}(700)$ (spread)
North Atl. Subpolar gyre	$1.7\ 10^{-4}$ ($0.5\ 10^{-4}$)	-	-
North Polar Front	$2\ 10^{-4}$ ($0.5\ 10^{-4}$)	$2.9\ 10^{-4}$ ($0.65\ 10^{-4}$)	$3.6\ 10^{-4}$ ($0.6\ 10^{-4}$)
South Polar Front	$1.7\ 10^{-4}$ ($0.6\ 10^{-4}$)	$2.4\ 10^{-4}$ ($1\ 10^{-4}$)	$2.4\ 10^{-4}$ ($0.6\ 10^{-4}$)
North Atl. Subtropical gyre	$1.7\ 10^{-4}$ ($0.5\ 10^{-4}$)	-	-
Indian Ocean	-	$3.3\ 10^{-4}$ ($0.8\ 10^{-4}$)	$2.4\ 10^{-4}$ ($0.3\ 10^{-4}$)
Eastern Med. Sea	$2\ 10^{-4}$ ($0.4\ 10^{-4}$)	-	-
Western Med. Sea	$1.9\ 10^{-4}$ ($0.4\ 10^{-4}$)	-	-

Results are presented in Table 2 for regions in which we had at least 10 profiles from three distinct floats per month. Specifically, we divided the Southern Ocean data set into two distinct zones, based on the local depth-averaged temperature between 190 and 210 m following *Swart and Speich* [2010] and *Pollard et al.* [2002]. Temperatures <6.5°C are representative of waters south of the Polar Front, while temperatures >6.5°C are representative of waters north of the Polar front. When we compute zonal statistics (Table 1), 2902 $b_{bp}(700)$ from floats that did not belong to any zone are lumped into one group. The distribution of all the measurements done with a given sensor type (Figure 2) suggests that $b_{bp}(700)$ is nearly normally distributed at depth, in contrast to particulate properties near the surface that are nearly log-normally distributed [*Campbell*, 1995; *Boss et al.*, 2013]. This result is likely due to the relative uniformity of concentrations at depth in contrast to the large and nonlinear change in surface concentrations, specifically in the productive regions of the ocean. In regions where different sensors types on floats have been deployed, we observed that a statistically significant differences existed between floats with ECO-Triplet (acceptance angle centered at 124°) from those measuring with Eco-FLBB (centered at 145°) or MCOMS (centered at 149°). We therefore separate the results according to each sensor used (Tables 1 and 2).

3. Results and Discussion

3.1. Median Value of $b_{bp}(700)$ Between 900 and 950 m

We find that different technologies provide significantly different estimates of median mesopelagic $b_{bp}(700)$, with the ECO-Triplet being the lowest, with a median of 1.8×10^{-4} m^{-1}, while the MCOMS and Eco-FLBB's median is about 2.8×10^{-4} m^{-1}, higher by about 50% (Table 1 and Figure 2). This difference is also observed, in general, at specific regions where all these technologies have been deployed on different floats (e.g., north and

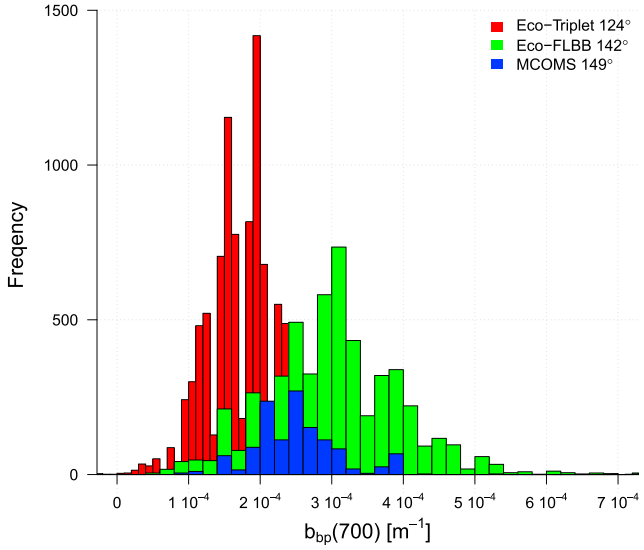

Figure 2. Histogram of median $b_{bp}(700)$ measured with each type of sensor for all profiles listed in Table 1.

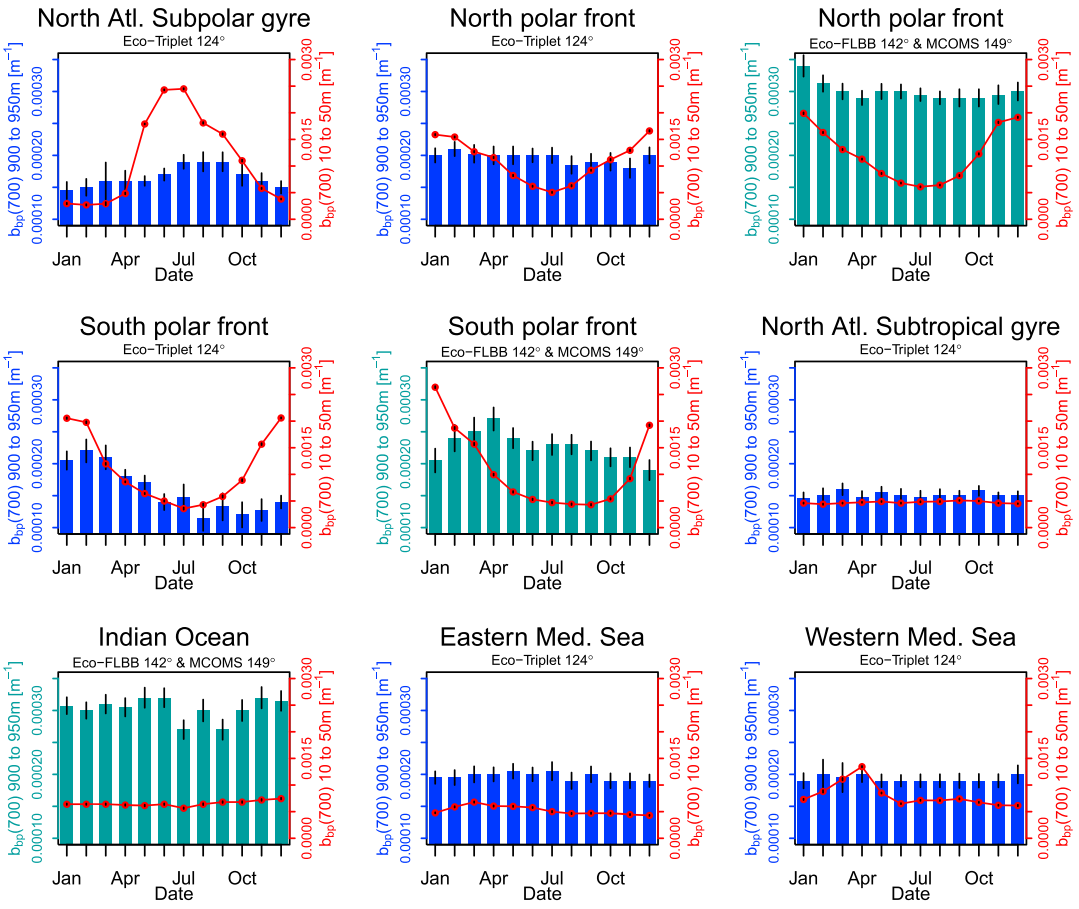

Figure 3. Histograms of monthly $b_{bp}(700)$ median values and resulting annual cycle at different oceanic regions with at least 10 profiles from three distinct floats per month, with blue denoting data with Eco-triplets and green combined Eco-FLBB and MCOMS at both surface (10–50 m, red lines) and 900–950 m. Black lines represent the spread of the median.

south of the Southern Ocean's Polar front). These differences cannot be explained solely based on our current understanding of the uncertainties in the conversion of measurements at one angle in the back direction and the backscattering coefficient (less than 10%) [e.g., *Boss and Pegau*, 2001, *Sullivan et al.*, 2013], or based on the difference of factory and on-the-float measured dark counts (see below). Nevertheless, variability within each region is smaller than 1×10^{-4} m^{-1} while the difference in the median value between regions for a given technology is smaller than 2.5×10^{-4} m^{-1} (Table 1). This attests to the relative stability of particulate concentration at this depth horizon. We have discovered through the years that the dark currents measured on floats are different from those provided by the sensor manufacturer. When we compared the differences for all the floats and sensor types for which we have access to such data ($N = 76$), we find that the median of factory darks underestimate the median of darks made on floats by 3 counts on average (48 versus 51), which represents a potential bias of 0.000035 m^{-1}. Removal of this possible bias would have made the data more consistent in particular with past values in the North Atlantic (see below).

3.2. Spatial Distribution of $b_{bp}(700)$ Between 900 and 950 m

Between zones where a large number of floats equipped with a given sensor have been deployed we find no significant differences in $b_{bp}(700)$ (Table 2). The exception is the Indian Ocean where most of the floats were deployed at a region with anoxic/suboxic sub-surface conditions. In such zones particulate material is less respired [*Roullier et al.*, 2014], as well as locally produced [*Morrison et al.*, 1999] consistent with the elevation of particulate concentration [*Whitmire et al.*, 2009]. This is also the likely reason why the few floats deployed in the Black Sea show high $b_{bp}(700)$ values (Table 1). Besides these specific areas, an explanation for the relative consistency in value at depth is that the deep particles are likely dominated by a background of refractory material.

3.3. Seasonal Dynamics $b_{bp}(700)$ Between 900 and 950 m

An annual cycle at depth is observed at the Southern Ocean polar front and North Atlantic, region with the largest amplitude in the seasonal cycles (Figure 3). There seems to be about 2 months delay between peak surface $b_{bp}(700)$ and peak $b_{bp}(700)$ at the 900–950 m depth (Figure 3), which suggests that the background concentration of particles at depth (which we quantify using the median operator) is likely mostly affected by small particle settling (large aggregates and particles settle at rates of 100 m per day). However, we note that disaggregation of large particles can also affect the background concentration. The annual cycle is absent at other regions (e.g., Mediterranean basins, North Atlantic subtropical gyre, and Indian Ocean). The variability of particle concentration of each month (computed using the spread of the median) appears to be nearly constant throughout the year at one location and between locations (Figure 3). Despite the significant differences in $b_{bp}(700)$ between sensors, we find the measured values to be consistent with past measurements of suspended particulate at depth; *Brewer et al.* [1976] report values varying from 5 to 20 μg/kg between 900 and 1000 m [*Brewer et al.*, 1976, Figure 1] in the North Atlantic. Assuming a specific attenuation coefficient at 660 nm of 0.8 m^2/mg and a specific backscattering coefficient at 660 nm of 0.008 m^2 mg^{-1}, *Boss et al.* [2015] predicted that the range of beam attenuation measured in such waters will be 0.005–0.015 m^{-1} while that for backscattering will be 5–15 $\times 10^{-5}$ m^{-1}. Uncertainties in these conversion factors are expected to be on the order 100% [*Hill et al.*, 2011; *Neukermans et al.*, 2012]. While these values are small relative to the accuracy of current technology, we find them to be of similar magnitude (though lower) relative to the values we report here (but given our uncertainties they are not significantly different). Many practitioners, e.g., *Gardner et al.* [2006] and references therein, not having appropriate calibration facilities on research vessels, prefer to use the minimal value at depths of several hundreds of meter as a reference for the rest of the water column. In this manuscript, using data acquired with commercially available backscattering sensors, we demonstrate their ability to resolve seasonal variations on the order of ~0.00001 m^{-1} equivalent to a change of about 1 ± 0.5μg kg^{-1} in suspended particulate matter, and, in addition, we are able to significantly resolve a positive signal of particles at depth.

4. Summary

We find the background $b_{bp}(700)$ measurements between 900 and 950 m to be relatively constant throughout most of the world's ocean and consistent with particulate mass concentration measurements performed in the 70s. Seasonal dynamics is nearly absent at depth except in regions with large seasonal variability at the surface. Observations of significant deviations from this value are therefore indicative of a regions where extraordinary processes take place or of a malfunctioning sensor. We found different technologies designed to estimate the particulate backscattering coefficient at 700 nm to differ significantly. Resolving this issue requires further investment in sensor characterization and/or in the study of the assumptions made regarding the behavior of particulate angular scattering (which at 900–950 m, could be significantly different from near-surface observations).

The Biogeochemical-Argo (BGC-Argo) program is progressively gaining maturity with a long-term vision of a sustainable global network [*Biogeochemical-Argo Planning Group*, 2016; *Johnson and Claustre*, 2016]. This paper is, to our knowledge, the first illustrating the benefits of access to a "global" BGC-Argo database. Furthermore, as BGC-Argo expands we hope to revisit these data and link them to the dynamics of ocean biology (chlorophyll, backscattering, and PAR (Photosynthetically Available Radiation)) and biogeochemistry (nitrate and oxygen evolution, pH), to better constrain the processes determining particle concentrations at depth and how these concentrations reflect global upper-ocean processes and their change.

Acknowledgments
The authors would like to acknowledge the support from NASA's Ocean Biology and Biogeochemistry program, the remOcean ("remotely-sensed biogeochemical cycles in the Ocean") project funded by the European Research Council (grant 246777) and the NAOS project (grant ANR J11R107-F). These data were collected and made freely available by the International Argo Program and the national programs that contribute to it: (http://www.argo.ucsd.edu, http://argo.jcommops.org). The Argo Program is part of the Global Ocean Observing System. The authors wish to thank the Argo Data Management team (ADMT) and the BGC Argo Data Management team (BGC ADMT) and in particular Catherine Schmechtig. We are grateful to Wilfrid Garner and to one anonymous reviewer for his valuable comments and suggestions. The authors also acknowledge the valuable comments and suggestions of Nathan Briggs, Henry Biting, Emanuele Organelli, and Alexandre Mignot.

References

Argo (2017), Argo float data and metadata from Global Data Assembly Centre (Argo GDAC) — Snapshot of Argo GDAC of March, 8st 2017, doi:10.17882/42182.

Biogeochemical-Argo Planning Group (2016), The scientific rationale, design and implementation plan for a Biogeochemical-Argo float array, doi:10.13155/46601.

Biscaye, P. E., and S. L. Eittreim (1977), Suspended particulate loads and transports in the nepheloid layer of the abyssal Atlantic Ocean, *Mar. Geol.*, *23*(1–2), 155–172.

Boss, E., and W. S. Pegau (2001), Relationship of light scattering at an angle in the backward direction to the backscattering coefficient, *Appl. Opt.*, *40*(30), 5503–5507.

Boss, E., D. Swift, L. Taylor, P. Brickley, R. Zaneveld, S. Riser, M. J. Perry, and P. G. Strutton (2008), Observations of pigment and particle distributions in the western North Atlantic from an autonomous float and ocean color satellite, *Limnol. Oceanogr.*, *53*(5), 2112–2122.

Boss, E., M. Picheral, T. Leeuw, A. Chase, E. Karsenti, G. Gorsky, L. Taylor, W. Slade, J. Ras, and H. Claustre (2013), The characteristics of particulate absorption, scattering and attenuation coefficients in the surface ocean; Contribution of the Tara Oceans expedition, *Methods Oceanogr.*, *7*, 52–62, doi:10.1016/j.mio.2013.11.002.

Boss, E., L. Guidi, M. J. Richardson, L. Stemmann, W. Gardner, J. K. Bishop, R. F. Anderson, and R. M. Sherrell (2015), Optical techniques for remote and in-situ characterization of particles pertinent to GEOTRACES, *Prog. Oceanogr.*, *133*, 43–54, doi:10.1016/j.pocean.2014.09.007.

Brewer, P. G., D. W. Spencer, P. E. Biscaye, A. Hanley, P. L. Sachs, C. L. Smith, S. Kadar, and J. Fredericks (1976), The distribution of particulate matter in the Atlantic Ocean, *Earth Planet. Sci. Lett.*, *32*(2), 393–402.

Campbell, J. W. (1995), The lognormal distribution as a model for bio-optical variability in the sea, *J. Geophys. Res.*, *100*(C7), 13,237–13,254.

Ewing, M., and E. M. Thorndike (1965a), Suspended matter in deep ocean water, *Science*, *147*(3663), 1291–1294.

Gardner, W. D., A. V. Mishonov, and M. J. Richardson (2006), Global POC concentrations from in-situ and satellite data, *Deep Sea Res., Part II*, *53*(5), 718–740, doi:10.1016/j.dsr2.2006.01.029.

Gardner, W. D., B. E. Tucholke, M. J. Richardson, and P. E. Biscaye (2017), Benthic storms, nepheloid layers, and linkage with upper ocean dynamics in the western North Atlantic, *Mar. Geol.*, *385*, 304–327, doi:10.1016/j.margeo.2016.12.012.

Hill, P. S., E. Boss, J. P. Newgard, B. A. Law, and T. G. Milligan (2011), Observations of the sensitivity of beam attenuation to particle size in a coastal bottom boundary layer, *J. Geophys. Res.*, *116*, C02023, doi:10.1029/2010JC006539.

Johnson, K. S., and H. Claustre (2016), Bringing biogeochemistry into the argo age, *Eos*, *97*, doi:10.1029/2016EO062427.

Morrison, J. M., et al. (1999), The oxygen minimum zone in the Arabian Sea during 1995, *Deep Sea Res., Part II*, *46*(8), 1903–1931, doi:10.1016/S0967-0645(02)00084-X.

Neukermans, G., H. Loisel, X. Méiaux, R. Astoreca, and D. McKee (2012), In situ variability of mass-specific beam attenuation and backscattering of marine particles with respect to particle size, density, and composition, *Limnol. Oceanogr.*, *57*(1), 24–144, doi:10.4319/lo.2011.57.1.0124.

Pollard, R. T., M. I. Lucas, and J. F. Read (2002), Physical controls on biogeochemical zonation in the Southern Ocean, *Deep Sea Res., Part II*, *49*(16), 3289–3305, doi:10.1016/S0967-0645(02)00084-X.

Roullier, F., L. Berline, L. Guidi, X. Durrieu De Madron, M. Picheral, A. Sciandra, S. Pesant, and L. Stemmann (2014), Particle size distribution and estimated carbon flux across the arabian sea oxygen minimum zone, *Biogeosciences*, *11*(16), 4541–4557, doi:10.5194/bg-11-4541-2014.

Schmechtig, C., A. Poteau, H. Claustre, F. D'Ortenzio, G. Dall'Olmo, and E. Boss (2015), Processing Bio-Argo particle backscattering at the DAC level, doi:10.13155/39459.

Sullivan, J. M., M. S. Twardowski, J. Ronald, V. Zaneveld, and C. C. Moore (2013), Measuring optical backscattering in water, in *Light Scattering Reviews 7*, edited by A. A. Kokhanovsky, pp. 189–224, Springer, Berlin, doi:10.1007/978-3-642-21907-8.

Swart, S., and S. Speich (2010), An altimetry-based gravest empirical mode south of Africa: 2. Dynamic nature of the Antarctic Circumpolar Current fronts, *J. Geophys. Res.*, *115*, C03003, doi:10.1029/2009JC005300.

Whitmire, A. L., R. M. Letelier, V. Villagrán, and O. Ulloa (2009), Autonomous observations of in vivo fluorescence and particle backscattering in an oceanic oxygen minimum zone, *Opt. Express*, *17*(24), 21,992–22,004.